Coordinated Neuronal Activity Enhances Corticocortical Communication

Highlights

- V2 spiking is preceded by epochs of enhanced V1 spiking coordination

- Coordinated spiking events do not propagate past direct downstream target networks

- Spiking coordination enhances corticocortical signaling in the visual system

Authors

Amin Zandvakili, Adam Kohn

Correspondence

zandvakili@gmail.com (A.Z.),
adam.kohn@einstein.yu.edu (A.K.)

In Brief

Cortical function requires communication between distinct areas. The importance of temporal coordination of spiking activity in this signaling has been debated. Zandvakili and Kohn show that coordination enhances communication between specific networks in primate areas V1 and V2.

Article

Coordinated Neuronal Activity Enhances Corticocortical Communication

Amin Zandvakili[1,*] and Adam Kohn[1,2,3,*]
[1]Dominick Purpura Department of Neuroscience
[2]Department of Ophthalmology and Visual Sciences
[3]Department of Systems and Computational Biology
Albert Einstein College of Medicine, Bronx, NY 10461, USA
*Correspondence: zandvakili@gmail.com (A.Z.), adam.kohn@einstein.yu.edu (A.K.)
http://dx.doi.org/10.1016/j.neuron.2015.07.026

SUMMARY

Relaying neural signals between cortical areas is central to cognition and sensory processing. The temporal coordination of activity in a source population has been suggested to determine corticocortical signaling efficacy, but others have argued that coordination is functionally irrelevant. We reasoned that if coordination significantly influenced signaling, spiking in downstream networks should be preceded by transiently elevated coordination in a source population. We developed a metric to quantify network coordination in brief epochs, and applied it to simultaneous recordings of neuronal populations in cortical areas V1 and V2 of the macaque monkey. Spiking in the input layers of V2 was preceded by brief epochs of elevated V1 coordination, but this was not the case in other layers of V2. Our results indicate that V1 coordination influences its signaling to direct downstream targets, but that coordinated V1 epochs do not propagate through multiple downstream networks as in some corticocortical signaling schemes.

INTRODUCTION

Cortical processing involves neurons distributed across distinct areas. These neurons must communicate by relaying signals through feedforward, feedback, and lateral pathways. The temporal coordination of activity in a source network has been suggested to strongly influence its efficacy in driving target networks through these corticocortical pathways (Singer and Gray, 1995; Fries, 2009). Further, computational modeling of multilayered, feedforward networks (FFNs) has shown that brief "packets" of synchronous spikes are a particularly effective signaling mechanism for some architectures (Diesmann et al., 1999; Litvak et al., 2003; Kumar et al., 2008, 2010). In the most extreme scenario—the "synfire" model—communication is achieved entirely through synchronous spikes, which propagate through multiple downstream networks (Abeles, 1991). However, in other models, signaling is achieved through rate fluctuations alone (Shadlen

and Newsome, 1998), and spike packets are ineffective (Vogels and Abbott, 2005).

The diversity of conclusions in modeling studies arises, in part, because the relevance of spiking coordination for corticocortical signaling depends on numerous factors, which remain poorly understood. These factors include the strength and precision of coordination in a source population, the coordination of excitation and inhibition, the degree of anatomical convergence and divergence between areas, and the integrative properties of downstream neurons (including the degree to which they operate in a fluctuation- or mean-driven regime; Salinas and Sejnowski, 2001; Kumar et al., 2010; Ratté et al., 2013). For instance, Salinas and Sejnowski (2000) showed that greater coordination among excitatory inputs does not lead to more spiking in a target neuron, when these inputs are also correlated with the inhibitory drive (see also Renart et al., 2010). Corticocortical signaling involves excitatory neurons, but their activity is tightly linked to downstream inhibition (Wehr and Zador, 2003; Gabernet et al., 2005). Thus, coordinated events in a source population may recruit substantial feedforward inhibition, quenching any advantage afforded by simple temporal summation of excitatory inputs.

Experimental work in the thalamocortical pathway has shown that pairwise synchronous spikes in the thalamus provide potent input to cortex (Alonso et al., 1996; Roy and Alloway 2001). Other studies have shown that cortical neurons may require synchronous convergent input from the thalamus to reach spiking threshold (Bruno and Sakmann 2006; Wang et al., 2010; Cardin et al., 2010). Studies of corticocortical signaling have shown interareal coordination of local field potentials, field-spike interactions (e.g., Salazar et al., 2012; Bosman et al., 2012; Roberts et al., 2013; van Kerkoerle et al., 2014), or pairwise spiking correlation (e.g., Nowak et al., 1999; Roe and Ts'o, 1999; Jia et al., 2013), often in specific frequency bands. These measurements provide important information about the relationship of neural activity across areas. However, local field potentials provide an indirect measure of spiking activity (Jia et al., 2011), and interareal pairwise spiking measurements cannot detect fluctuations in population coordination. Further, in previous work, recordings were often made without knowledge of the laminar location of the target and source neurons, which we show here can strongly influence inferences about corticocortical communication. Thus, despite the central role of spiking coordination in many corticocortical signaling schemes, it remains unclear
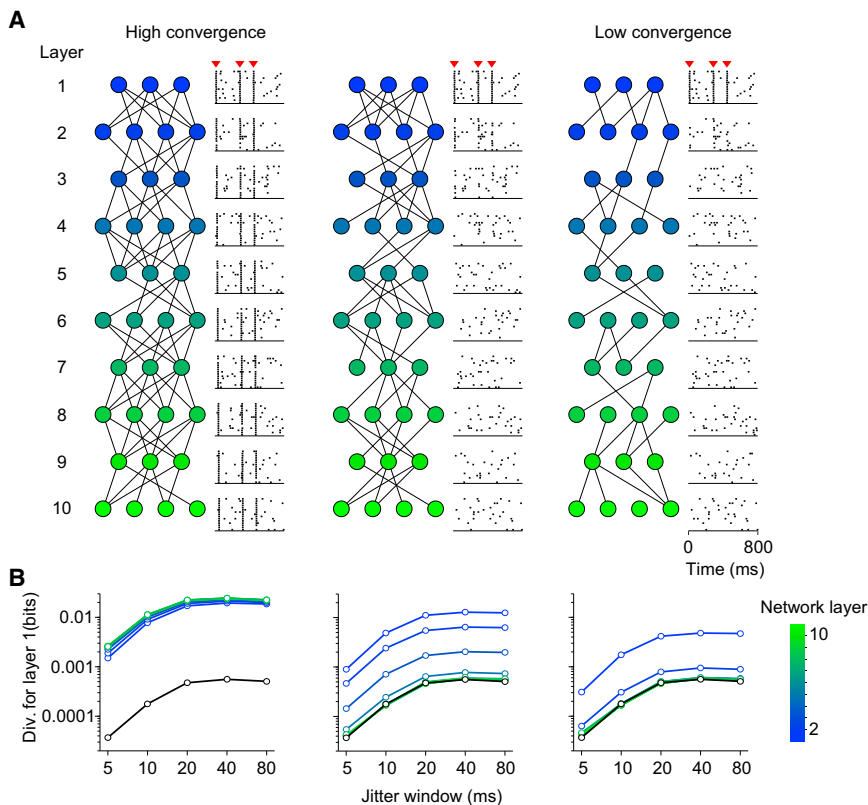
Figure 1. Propagation of Spike "Packets" in FFNs

(A) Activity in a multilayer FFN of excitatory integrate-and-fire cells. The rasters illustrate the activity of a population of neurons, in a brief epoch of time. Coordinated epochs (marked by red arrowheads) propagate through densely interconnected networks (left), but not sparsely interconnected ones (center, moderate convergence; right, sparse convergence).

(B) Divergence values in the first layer, using either random epochs (black line) or epochs associated with spikes in layers two through ten (blue to green colors, as indicated). For each layer, divergence values are calculated using layer 1 responses, in epochs that take into to account the slight delay for activity to reach deeper layers.

Experimental Procedures) and its behavior entirely consistent with the description of that study.

In the first FFN variant (Figure 1A, left), there is high convergence of inputs from one level of the network to the next. In this architecture, spike packets in layer 1 (arrow heads in population activity rasters, see Experimental Procedures) are effective at driving neurons in layer 2, which in turn drive neurons at the next level. Spike packets propagate through the entire network, and are evident at the deepest layers (layer 10, light green). This behavior is consistent with "synfire" signaling schemes (Abeles, 1991), which have received some experimental support in the songbird (Long et al., 2010) and the cortical slice preparation (Reyes, 2003). In contrast, the same spike packets in layer 1 fail to propagate in a FFN with low convergence (Figure 1A, right). Networks with intermediate convergence (middle) have intermediate propagation properties. In these simulations, the propagation of spike packets is determined by convergence but, as noted previously, it also depends on numerous other factors.

In FFN models, the propagation efficacy of packets is typically measured by comparing their amplitude (i.e., the number of neurons involved) and temporal dispersion across layers (Diesmann et al., 1999; Kumar et al., 2008, 2010). This measurement is not easily applied in vivo, where specific activity patterns are diverse, generated spontaneously, and may rarely be repeated (Okun et al., 2012). An alternative is to quantify the relationship between firing in downstream networks and the strength of coordination in a relevant upstream network: if spike packets are important for signaling, then downstream spiking should be preceded by heightened coordination in a source network. Note that an additional advantage of this measure is that it implicitly considers the rate of occurrence of spike packets. If these occur rarely, there will be little functional relevance for downstream networks, even if such events provide potent input.

Existing metrics do not capture moment-to-moment changes in coordination. Cross-correlograms (CCGs), for instance, are computed across trials, and thus cannot identify epochs of
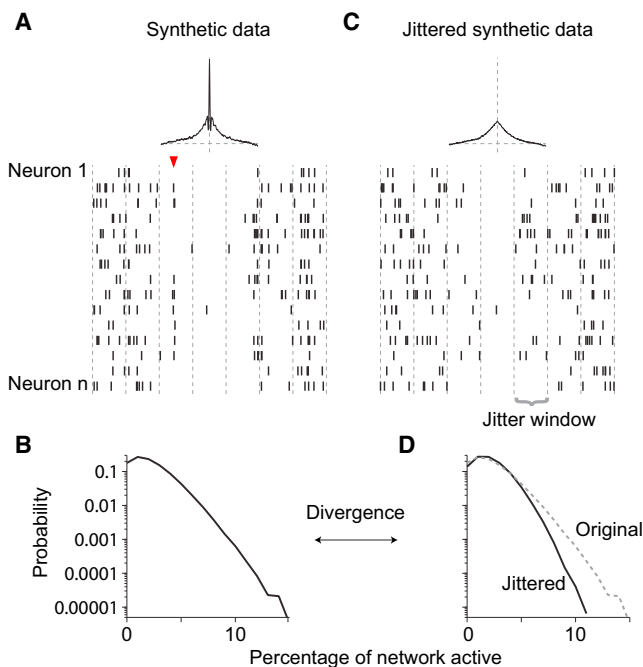
how coordination in a source population influences its efficacy in driving downstream networks.

Here we test how the coordination of spiking activity in the output layers of primary visual cortex (V1) is related to spiking activity in V2. We reasoned that if V1 coordination were important for relaying signals, V2 spiking should be preceded by epochs of greater V1 coordination. We developed a metric to quantify V1 coordination on an epoch-to-epoch basis. This analysis revealed that spiking activity in the input layers of V2 is preceded by markedly elevated V1 coordination, strongly suggesting that coordination enhances corticocortical signaling. However, spiking in other layers of V2 was not related to V1 coordination, ruling out signaling schemes in which coordinated spiking events in a source area propagate through multiple downstream networks.

RESULTS

To motivate our approach, we first consider the efficacy of coordinated spiking events (or spike "packets") in relaying signals through three variants of a FFN. FFNs are broadly relevant for understanding the relaying of neuronal activity, as other network architectures (e.g., recurrent networks) can be decomposed into a sequence of FFNs (Goldman, 2009). Our FFN consisted of multiple populations of leaky integrate-and-fire neurons, organized in discrete layers (Figure 1A). Each layer provides input to a downstream network, which receives additional input from an independent pool of neurons (not shown). Our model is nearly identical to that implemented by Diesmann et al. (1999) (see

Figure 2. Using Jensen-Shannon Divergence to Measure Population Coordination

(A) Raster of activity of 15 correlated cells. The average pairwise CCG of the cells in the full population (n = 100) is plotted above the raster. The red arrowhead indicates a synchronous spiking event involving several cells.

(B) The probability distribution that the indicated percentage of the network (abscissa) is active in a 1 ms bin.

(C) Jittered version of the population on the left. The jitter window is marked by vertical lines. Average pairwise CCG indicated at top; note the disappearance of precise temporal synchrony.

(D) The activity distribution of the jittered (solid line) and original (dotted line; replotted from B) population. Coordination is quantified as the divergence between the original and jittered distributions.

enhanced coordination if these are not stimulus-locked. In addition, CCGs only measure pairwise correlations. This is a critical limitation as a change in higher-order correlations, for a fixed level of pairwise correlations, can greatly alter the summed input provided to downstream networks (Kuhn et al., 2003).

We therefore developed a new metric to quantify population coordination. We first illustrate its properties with synthetic data. These data were generated using an established algorithm for producing population responses with specified pairwise correlations (Macke et al., 2009), which we modified to produce correlations involving a range of timescales (see Experimental Procedures). The activity in our synthetic population was coordinated on both brief (Figure 2A, red arrowhead) and long timescales, resulting in an average CCG (Figure 2A, top) that mimics those typically seen in V1 (Smith and Kohn, 2008).

To quantify population coordination, we first calculated the probability distribution of network "states" (Figure 2B). These states are defined as the percentage of the network that is active in a 1 ms window. The shape of the resultant distribution reflects both the firing rate of individual neurons and the degree to which activity is coordinated (including pairwise and higher-order cor-

relations). Higher firing rates would shift the distribution to the right; for a given firing rate, more coordination would lead to higher distribution kurtosis—that is, more periods in which much of the network is either quiescent or active.

To isolate the contribution of coordination, we compared the measured distribution with that of surrogate data. These data were created by defining a "jitter" window (i.e., a time bin) and then, for each spike on each trial, choosing a new spike with replacement from the set of all spikes that the neuron fired in the same bin on other trials (Smith and Kohn, 2008). In this way, the individual neuronal firing rates in the jittered and raw data are identical, and the spike count of each neuron in each jitter window and on each trial is maintained. Jittering thus preserves entirely the first-, second-, and higher-order statistics of the original population response, but removes all second- and higher-order structure on timescales shorter than the jitter window. The effect of jittering is evident in the population raster (Figure 2C; jitter window 640 ms), in which the synchronous event of Figure 2A has been destroyed. Jittering thus changes the distribution of network states (Figure 2D). For instance, events in which 10% of the population fired together occurred with a probability of roughly 0.001 (i.e., once per second) in the original data (Figure 2B), but were 100-fold rarer in the jittered data (Figure 2D).

We quantified the difference between the original distribution and that based on jittered data using Jensen-Shannon divergence (D_{JS}; see Experimental Procedures), a standard measure of the difference between two probability distributions. For a given population size and number of samples, a larger divergence indicates greater population coordination on a timescale shorter than the jitter window. To confirm this, we generated synthetic responses for 100 neurons with pairwise correlations varying from 0.05 to 0.2, as often seen in cortex (Cohen and Kohn, 2011). Correlations were due to both brief and long timescale coordination. Increasing correlations from 0.1 (Figure 3A, green) to 0.2 (red) caused a roughly 3-fold increase in divergence; reducing correlations from 0.1 to 0.05 (blue) caused a 3-fold decrease in divergence, across a wide range of jitter windows. For each correlation strength, divergence increases with the size of the jitter window because larger windows remove progressively longer timescales of correlations, causing the surrogate distribution to match the original data less closely. In additional analysis, we confirmed that divergence is also sensitive to a change in higher-order response correlations, when pairwise correlations are kept constant (see Figure S1 available online). Importantly, divergence was not sensitive to wide variations in the firing rate of individual neurons in the population (Figure 3B).

When applied to the FFNs of Figure 1, our divergence metric captures the propagation efficacy of spike packets. The average coordination in layer 1 is captured by computing the divergence using all response epochs (Figure 1B, black line). Because our spike packets had a temporal precision of ~15 ms, the divergence values increase with jitter window size up to this value and then asymptote. The blue to green lines in Figure 1B indicate the divergence in layer 1, in epochs preceding downstream spiking of each subsequent layer (with a slightly different temporal offset to account for propagation delays across layers of the network). For networks in which spike packets readily propagate
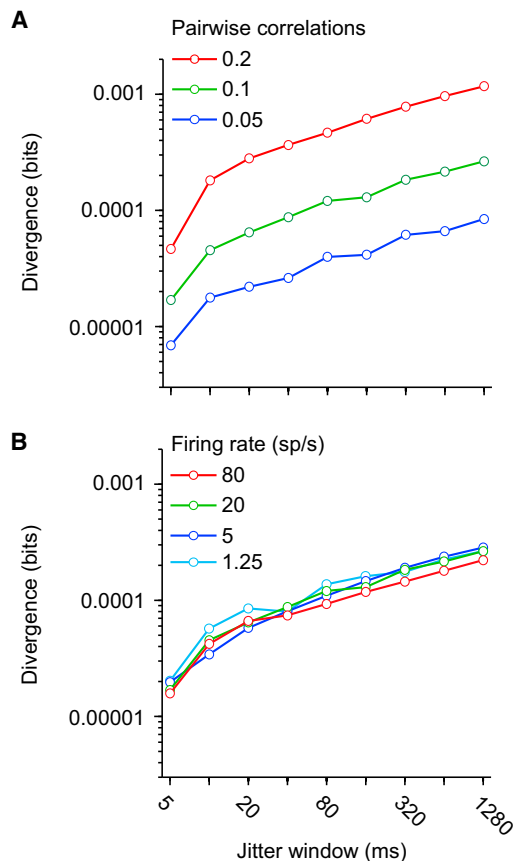
A

Pairwise correlations

B

Firing rate (sp/s)

Figure 3. Dependence of Divergence on Pairwise Correlations and Neuronal Firing Rate

(A) Divergence values calculated between original and jittered populations, for jitter windows ranging from 5 to 1,280 ms and for populations (n = 100) with mean pairwise correlations of 0.05 (blue), 0.1 (green), and 0.2 (red). The spike count correlation values were calculated in 1 s epochs. The average firing rate of the neurons was 20 sp/s.

(B) Divergence values for populations firing at 1.25, 5, 20, or 80 sp/s. Correlations were fixed at 0.1.

A

B

C

Figure 4. Targeting Downstream Networks Receiving Direct V1 Input

(A) Schematic showing a sagittal section of occipital cortex and the arrangement of the recording apparatus. Inset shows a Nissl-stained section of V2 from one animal, with the site of an electrolytic lesion indicated by the arrowhead. Scale bar, 1 mm.

(B) RF centers for each V1 (blue dots) and V2 (red) electrode from one recording session. The blue and red disks indicate the extent of example RFs for two V1 neurons and one V2 neuron. The spatial configuration of the RFs reflects the physical arrangement of the recording electrodes in V1 (a grid) and V2 (a linear array).

(C) (Left) V1-V2 CCGs recorded at 10 V2 recording sites along a sequential, translaminar penetration, calculating by averaging CCGs from all simultaneously recorded pairs at each site. Number of pairs at each site varied from 672 to 1,680. (Right) Same V1-V2 CCGs after jitter correction (jitter window of 10 ms). Significant CCGs are indicated by red arrow.

(Figure 1B; left), the layer 1 divergence is consistently elevated regardless of which downstream layer defines the relevant epochs. For instance, a spike in layer 10 is preceded by greater divergence within layer 1 (green line) than observed on average in layer 1 (black line), because some of the downstream spikes are preceded by synchronous events within layer 1. In contrast, in networks in which spike packets fail to propagate (Figure 1B, right), the divergence values within layer 1 quickly converge to those seen on average in that layer (black line). Thus, beyond layers 2 or 3, downstream spiking is not associated with heightened coordination in layer 1, indicating a failure of spike packets to propagate.

In summary, the divergence between an empirical and jittered distribution of network states captures the strength of population coordination—including, but not limited to, changes in pairwise correlations. This metric allows one to measure networks coordination in arbitrary epochs, including those defined by an external event such as a spike in a downstream network.
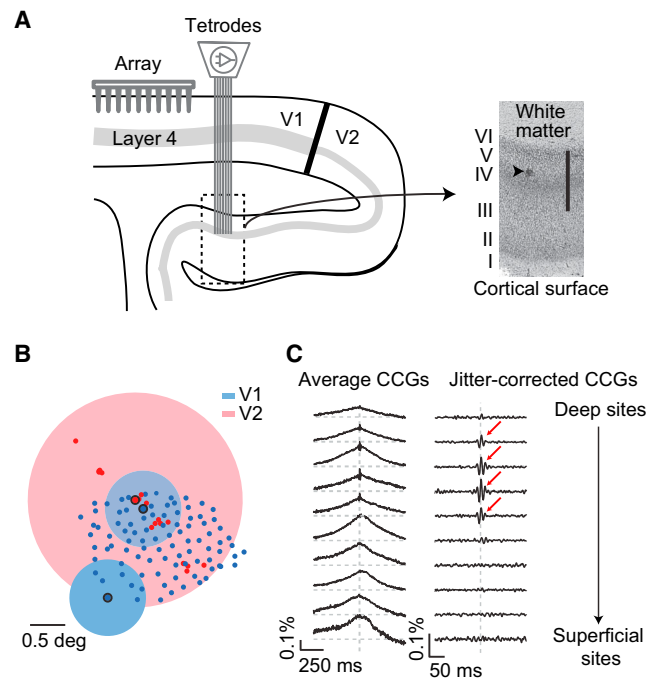
V1-V2 Recordings

With this framework at hand, we turned to measuring the influence of spiking coordination in relaying signals across stages of primate visual cortex. We focused on the circuit linking V1 and V2, which is one of the most extensive feedforward circuits in primate neocortex, with well-studied anatomy (Felleman and Van Essen 1991). In addition, V1 is known to be the principal source of input to V2: cooling or lesioning V1 abolishes most (Schmid et al., 2009) or all (Girard and Bullier, 1989) evoked activity in V2.

We recorded from V1 using a 96-channel array implanted to a nominal depth of 600 microns. The electrode length (1 mm) ensured that our recordings were limited to layers 2/3 and 4B, which project to higher cortex (Felleman and Van Essen, 1991). We paired our V1 measurements with V2 recordings, using translaminar penetrations with a set of moveable electrodes and tetrodes (Figure 4A). In both areas, we analyzed well-isolated single units and small cluster of such units, and pooled
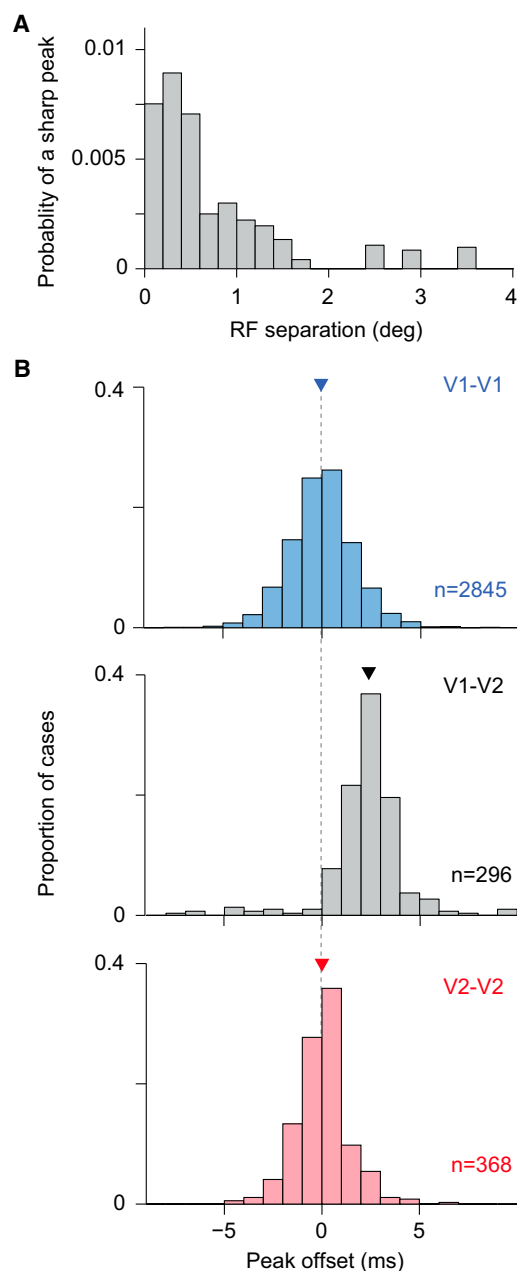
Figure 5. Properties of Narrow V1-V2 CCG Peaks

(A) The probability of finding a significant narrow CCG peak, as a function of V1-V2 RF separation (center-to-center distance).

(B) Temporal offset of the narrow V1-V1 (blue), V1-V2 (gray), and V2-V2 (red) CCG peaks. Only pairs with significant peaks are included. Thin vertical line is to facilitate comparison. Arrowheads indicate medians.

centers of the V1 (blue circles) and V2 (red) RFs for one example recording session, with the size of three example RFs indicated by shading (mean diameter of 1.21° ± 0.01° (SEM) for V1 and 2.27° ± 0.05° for V2). In many cases, the V1 and V2 RFs were aligned within a fraction of a degree.

To understand how spiking activity in V1 and V2 is related, we first measured pairwise correlations at different laminar locations. We presented full-contrast drifting gratings of different orientations, whose size (typically 2°–3.5°) was sufficient to cover the RFs of units in both areas. From this driven activity, we computed CCGs between all simultaneously recorded V1-V2 pairs (see Experimental Procedures). We frequently observed broad peaks in V1-V2 CCGs, tens to hundreds of milliseconds wide. These were evident in the average V1-V2 CCGs at all laminar locations, as shown for a sample penetration (Figure 4C; left).

At a subset of V2 sites, we observed narrow CCG peaks (see also Smith et al., 2013; Jia et al., 2013). The narrow peaks can be seen most clearly in jitter-corrected CCGs (arrows in Figure 4C; right), which removes the broad component of the CCG (see Experimental Procedures). Average V1-V2 CCGs contained a significant narrow peak at 46 of 223 V2 sites, whose mean depth was 694 ± 49 (SEM) microns superficial to the layer 6/white matter border. Given our penetration angle, this is the expected depth of layer 4 and deep layer 3 (Figure 4A, inset), the termination site of V1 axons (Rockland and Virga, 1990). In three animals, we were able to confirm histologically that V2 sites with a narrow CCG peak were in or abutting layer 4 (Figure 4A, inset).

The probability of observing a significant narrow CCG peak also depended strongly on the center-to-center distance between the V1 and V2 spatial RFs. The probability was highest for pairs with offsets of <0.5°, and decayed quickly with greater offsets (Figure 5A). Even for pairs with well-aligned RFs, the probability was only ~1%. In total, 0.3% of V1-V2 pairs had a significant narrow peak (n = 296 out of 83,441 pairs). Thus, narrow CCG peaks were rare, and displayed striking specificity for laminar position of the V2 neuron and for the alignment of the V1 and V2 spatial RFs.

We next analyzed the temporal delay of narrow CCG peaks to determine if they were consistent with direct input from V1 to V2. Narrow peaks were offset from zero time lag by a median of 2.8 ms (Figure 5B, gray; p < 0.001 for difference with 0), with an average peak width of 3.71 ± 0.05 ms (SEM). Thus, there was an enhanced probability that the V2 cell would fire roughly 3 ms after a V1 spike, consistent with the conduction and synaptic delays for connections between V1 and V2 (Girard et al., 2001; El-Shamayleh et al., 2013). In contrast, significant peaks in V1-V1 (Figure 5B; blue, n = 2845) and V2-V2 (red, n = 368) jitter-corrected CCGs had a median offset of 0.0 ms (p = 0.45 and 0.42, respectively, for difference from zero). Further description of the magnitude and shape of the narrow V1-V2 CCG peaks is provided in Figure S3.

In summary, at V2 laminar locations where fibers from V1 are known to terminate, we found short-latency V1-V2 functional coupling, between pairs with well-aligned spatial RFs. Pairs with offset RFs, or in deeper or more superficial layers, did not show evidence of this coupling.
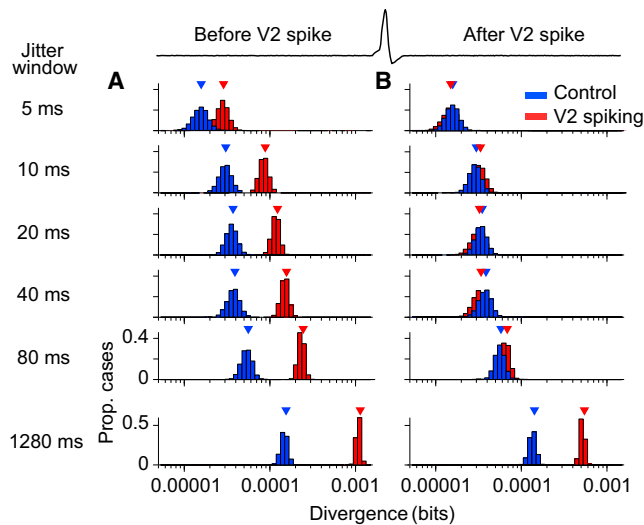
results using these two types of recordings. We obtained similar results when using only single units (Figure S2). In total we recorded 896 V2 cells in 7 monkeys, paired with V1 populations of 61–160 units (average 98).

We used anatomical landmarks and the topographic organization of V1 and V2 to target neurons in the two areas with overlapping spatial receptive fields (RFs). Figure 4B illustrates the

Figure 6. Activity of V2 Cells Is Associated with Elevated Coordination in V1

(A) Divergence values for the V1 population, calculated in control epochs (blue) and in epochs preceding a V2 spike (red) by 1.5–3.5 ms, for jitter windows ranging from 5 ms (top) to 1,280 ms (bottom). Distributions represent 5,000 bootstrap calculations of D_{JS}.

(B) Divergence values for the V1 population, in epochs 1.5–3.5 ms after a V2 spike. Conventions are as in (A).

V2 Spiking Is Preceded by Stronger V1 Coordination

To test the importance of network coordination for corticocortical signaling, we applied our divergence metric to our paired V1-V2 recordings. If V1 coordination is important for relaying signals downstream, V2 spiking should be preceded by enhanced V1 coordination. This enhancement would be evident as higher divergence values.

We first focused on middle-layer V2 sites, where neurons receive direct input from V1. These sites were defined by the presence of a significant narrow peak in the site-average V1-V2 CCG (see Experimental Procedures). We computed an average distribution of V1 network states, in epochs 1.5–3.5 ms before each spike of each V2 neuron at those sites (aggregating 3,846,629 epochs from 226 V2 neurons). We then calculated the divergence between this distribution and a surrogate distribution, computed from identical epochs using jittered responses. To obtain confidence intervals for the divergence, we used a bootstrap procedure: we resampled neurons with replacement from the set of relevant V2 sites, and computed divergence between each of the resultant distributions and the corresponding surrogate data.

Figure 6A shows the resultant divergence values (arrowheads) and bootstrap distributions in epochs preceding V2 spiking (red), for a range of jitter windows (different rows). These distributions indicate the strength of spiking coordination within V1, just before a V2 spike. How does this compare to the typical strength of V1 coordination? To address this, we quantified coordination in control epochs: for each V2 spike, we chose an epoch from another trial with identical timing with respect to stimulus onset. This choice ensured that the trial-average firing rate in V1 and V2

was matched for control epochs and epochs associated with spike in the V2 target neuron. We computed the divergence between V1 states in these control epochs, and the corresponding surrogate data. The divergence values in control epochs (blue) were significantly smaller than in epochs preceding V2 spiking (red; p = 0.011 for jitter window of 5 ms; p < 0.001 for all other jitter windows). Thus, in epochs preceding V2 spiking, V1 coordination was clearly elevated compared to control epochs.

In epochs 1.5–3.5 ms after the occurrence of a V2 spike, there was no difference in divergence with control epochs, for jitter windows between 5 and 80 ms (Figure 6B; p > 0.18 for all comparisons). Thus, V1 coordination was enhanced before but not after V2 spiking. For larger jitter windows, there was enhanced divergence both before and after V2 spiking, as illustrated for a jitter window of 1280 ms (red compared to blue; bottom row of Figures 6A and 6B; p < 0.001 for both cases). Thus, V2 spiking was both preceded and followed by elevated long-timescale correlation in V1, presumably because the fluctuations that give rise to long-timescale V1 correlations are long lasting. The significant difference in divergence after V2 spiking precludes an inference that V2 spiking is driven by fluctuations in V1 correlations on slow timescales. We therefore focused our remaining analysis on brief timescale coordination (jitter windows less than 80 ms).

For epochs 1.5–3.5 ms before V2 spiking, the mean divergence values are replotted in Figure 7A. Divergence values for epochs associated with V2 spiking were roughly 3-fold greater than in control epochs. How strong must V1 coordination be in these epochs to generate the observed difference with control epochs? The simulations of Figure 3, which used a matched population size and number of samples, indicate that an increase in divergence of this magnitude requires roughly a doubling of pairwise correlations, if there is no change in higher-order correlations. The enhancement of V1 coordination preceding V2 spikes was thus substantial. Note that both for epochs preceding V2 spiking and for control epochs, the divergence values were significantly larger than those obtained from shuffled data (Figure 7A, black). In shuffled data, a divergence between the empirical and jitter distributions can only be due to finite data, since shuffling removes correlations. Thus, V1 activity is coordinated during control epochs (blue compared to black), but the strength of this coordination is substantially smaller than in epochs preceding V2 spiking (red compared to blue).

We next determined the time course of elevated V1 coordination around the timing of V2 spiking. Figure 7D shows the difference in divergence between epochs associated with V2 spiking and control epochs, for a range of temporal offsets and jitter windows. Enhanced V1 coordination was evident several milliseconds before V2 spiking, but not in more temporally distant epochs or in epochs following V2 activity. These results strongly suggest that brief epochs of enhanced V1 coordination drive V2.

If coordinated V1 epochs propagate through multiple downstream networks—as in the high-convergence FFN of Figure 1—spiking activity in V2 layers that do not receive direct V1 input should also be preceded by elevated V1 coordination. That is, spike packets in V1 should propagate effectively through the middle layers of V2, and drive neurons further downstream in
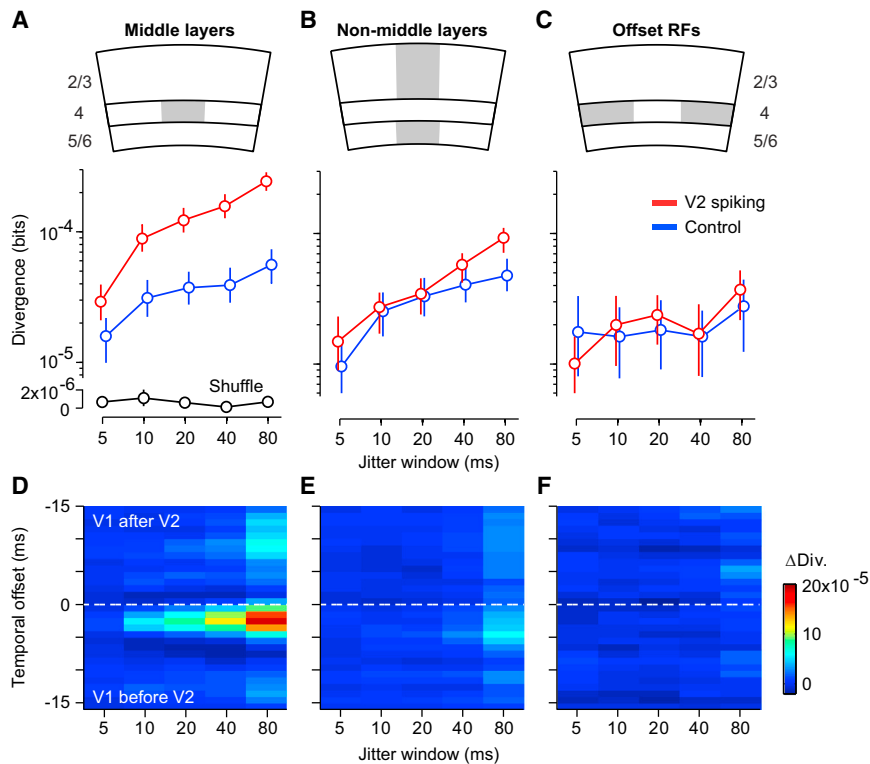
Figure 7. Relationship between V1 Coordination and Spiking Activity in Various V2 Neurons

(A) Divergence values conditioned on spikes occurring in middle-layer V2 neurons (red) or in control epochs (blue), for a range of jitter windows. Divergence values for shuffled data are shown for comparison (black). Error bars indicate 95% confidence intervals based on bootstrap, as explained in the text.

(B) Same as (A), but for neurons recorded at sites either superficial to or deeper than the middle layers.

(C) Same as (A) but for V2 neurons 500–1,000 microns from the layer 6/WM border, with offset receptive fields. Note V1 correlations on time-scales >5 ms were slightly weaker in these recordings, leading to smaller divergence values than in (A) and (B); divergence was also similar in epochs associated with V2 spiking and control epochs, when we used a subset of the data with stronger correlations (data not shown).

(D) Difference in divergence for epochs associated with spiking in a middle-layer V2 neuron and for control epochs, for a range of jitter windows and temporal offsets. The temporal offset is with respect to the timing of V2 spikes; time 0 is when the V2 spikes occurred. Color scale indicated on the right; higher divergence is shown by red.

(E) Same as (D), for V2 neurons recorded at sites above or below the middle layers.

(F) Same for V2 neurons with offset receptive fields.

the superficial and deep layers of V2. We therefore analyzed V1 coordination preceding V2 spiking recorded at sites either superficial or below those providing sites with narrow CCGs (n = 236 neurons; 2,398,161 epochs). In epochs 1.5–3.5 ms before V2 spikes in these layers, divergence was not significantly different from that measured in control epochs (Figure 7B; p = 0.008 for jitter window of 80 ms; p > 0.15 for other windows). We explored a range of temporal offsets relative to the V2 spikes, but the difference in divergence between epochs around the time of V2 spikes and control epochs was minimal (Figure 7E). Thus, in striking contrast to the middle layers of V2 (Figure 7D), there is no measurable difference in brief-timescale V1 coordination in epochs preceding the spiking activity of V2 neurons in superficial and deep layers.

Finally, we wished to determine whether the relationship between V2 spiking and V1 coordination was retinotopically specific. We analyzed epochs associated with the spiking activity of V2 neurons whose receptive fields were offset by at least 3° from the center of the V1 population (n = 80 neurons; 1,382,605 epochs). For these offsets, we could not use V1-V2 CCGs to detect the termination site of V1 inputs; instead we used V2 neurons recorded at depths where we had observed narrow peaks when the RFs were aligned (between 500 and 1,000 microns from the layer 6/white matter border). We found no difference in divergence in epochs associated with spiking of these V2 neurons, compared to control epochs (Figures 7C and 7F; p > 0.2 for all comparisons). Thus, the relationship between V2 activity and enhanced V1 coordination requires precise alignment of the receptive fields.

Dissociation of Divergence Analysis and Measurements of Pairwise Synchrony

We found that V1 coordination was enhanced in epochs preceding spiking activity in middle-layer V2 cells with retinotopically aligned RFs, but not for other V2 neurons. This specificity applies equally well to the presence of narrow V1-V2 CCG peaks—these were evident only in the appropriate layer of V2, when the RFs were well aligned. We thus wondered whether our finding of enhanced V1 coordination simply followed from the presence of significant V1-V2 pairwise spike timing correlations.

We conducted additional simulations in which we modeled a V2 neuron as a leaky, integrate-and-fire neuron, as in the FFNs of Figure 1. The V2 neuron received balanced excitatory and inhibitory drive from Poisson populations, as well as excitatory feedforward input from a correlated V1 population (Figure 8A; see Experimental Procedures). We sampled from a subset of the projection V1 population, and found the average V1-V2 CCGs had a narrow peak (Figure 8B). In addition, V1 coordination was elevated in epochs immediately preceding a V2 spike, compared to control epochs (Figure 8C; red compared to blue). Thus, this simulation recapitulated the effects in the data. Note that the enhanced coordination preceding a V2 spike—similar in magnitude to the enhancement observed physiologically—was evident in an integrate-and-fire neuron in the "fluctuation-driven" regime (i.e., receiving balanced excitatory and inhibitory input from many background neurons). No additional downstream selectivity for coordinated input, such as nonlinear synaptic integration (Jahnke et al., 2013), is required.
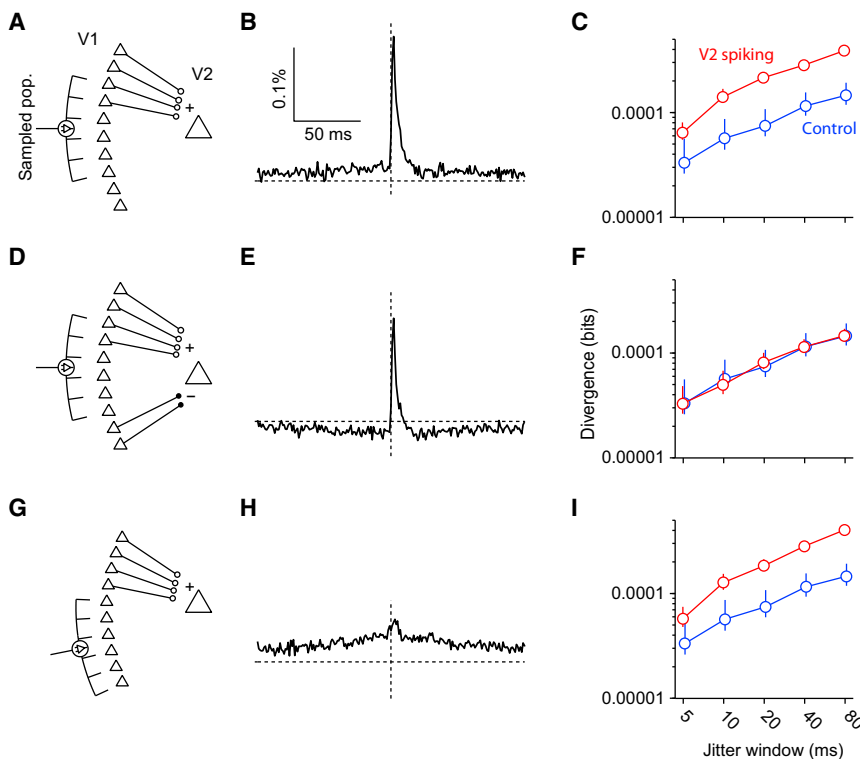
In a second scenario, the model V2 cell received both excitation and inhibition from the coordinated V1 population (Figure 8D). Inhibition was implemented by simply inverting the sign of the input provided by a subset of the V1 neurons. There was thus no delay between excitation and inhibition, approximating the rapid nature of feedforward inhibition (Wehr and Zador, 2003; Gabernet et al., 2005). In this network we also observed CCG peaks between excitatory V1 neurons and the V2 cell (Figure 8E), but V2 spiking was not preceded by elevated V1 coordination (Figure 8F). Thus, the presence of a CCG peak does not indicate that downstream spiking will be preceded by elevated coordination in the input population. Further, this simulation shows that firing of a downstream neuron in a FFN need not be related to the strength of coordination in its input. The absence of this relationship occurs because feedforward inhibition cancels the influence of coordinated excitatory input (Salinas and Sejnowski, 2000, 2001; Renart et al., 2010). If inhibition were delayed relative to excitation, this would generate a temporal window through which transient elevations of input correlation would drive the downstream neuron (Kremkow et al., 2010), effectively a high-pass filter. In this case, V2 activity would be associated with enhanced V1 coordination on brief but not long timescales (data not shown).

In the final scenario, we "recorded" the activity of V1 neurons which did not project to V2, but whose activity was coordinated with neurons that did project (Figure 8G). In this case, there was no peak in the V1-V2 CCG (Figure 8H). However, V1 coordination was greater in epochs preceding V2 spiking (Figure 8I). Divergence was elevated because a spike in the V2 neuron was preceded by greater coordination among the projection neurons,

which was in turn associated with coordinated activity in the recorded cells. Thus, it is not necessary to measure the spiking activity in all projection neurons to determine the relationship between network coordination and downstream spiking; rather, the recorded neurons need only be embedded, and correlated with, the relevant projection neurons. Consistent with this intuition, we found in the recorded data that V1 coordination was elevated before the spiking of retinotopically aligned, middle-layer V2 neurons, both for V2 neurons that had a significant CCG peak with a recorded V1 neuron and for those V2 neurons recorded at the same site that did not (Figure S4).

Together these three simulations illustrate that the presence of significant pairwise timing correlations (i.e., a significant interareal CCG peak) is neither necessary nor sufficient for determining whether downstream spiking is related to the strength of coordination in the input population. Further, these simulations show that the relationship between V2 spiking and V1 coordination is captured by an integrate-and-fire cell operating in the fluctuation-driven regime, and does not indicate synergistic summation of synaptic input in the downstream neuron.

DISCUSSION

We recorded simultaneously from neuronal populations in the output layers of V1, and from downstream V2 networks. We found that spiking in middle-layer V2 neurons was preceded by substantially elevated V1 spiking coordination, strongly suggesting that spike packets are a particularly effective corticocortical signaling mechanism. In contrast, V2 spiking outside the middle layers was not associated with enhanced V1 coordination. This failure of coordinated spiking events to propagate through multiple stages of downstream processing indicates that cortical communication does not involve serial propagation of synchronous events, as in a "synfire" network (Abeles, 1991; Reyes, 2003; Long et al., 2010).

Relation to Previous Work

Computational models have revealed that it is surprisingly difficult to relay signals through multiple layers of a FFN (Diesmann et al., 1999; Litvak et al., 2003; Vogels and Abbott, 2005; Kremkow et al., 2010; Kumar et al., 2008, 2010; Jahnke et al., 2013). Rate fluctuations in a source network often die out or lead to a fixed output in downstream networks (Litvak et al., 2003). Successful rate propagation requires sparse connectivity with strong synapses (Vogels and Abbott, 2005; Kumar et al., 2010). In contrast, synchronous events propagate successfully through multiple layers of a FFN (Diesmann et al., 1999; Kremkow et al., 2010; Kumar et al., 2008, 2010; Litvak et al., 2003), when these are connected by denser but weaker synapses (Kumar et al., 2010). However, when FFNs are embedded in recurrent networks, synchronous events can generate runaway, explosive activity in downstream networks (Mehring et al., 2003), and, for some network architectures, coordinated activity does not propagate as effectively as rate fluctuations (Vogels and Abbott, 2005).

Computational work has thus shown a wide range of possible corticocortical signaling regimes. Neurophysiological work has begun to elucidate the relationship of activity distributed across cortical areas, showing that it can be strengthened or weakened by various cognitive and sensory variables (e.g., Gregoriou et al., 2009; Salazar et al., 2012; Roberts et al., 2013). But this work has left unclear which signaling regime is most relevant for corticocortical communication. Here we determined the relationship between spiking in a downstream network and the coordination within an input population. To measure V1 coordination in epochs associated with V2 spiking, we used a "spike-triggered" approach, analogous to that used to characterize neuronal receptive fields (Schwartz et al., 2006). In our case, we quantified the strength of coordination within the V1 population, in epochs triggered by V2 spiking activity, and compared this coordination to that in control epochs. The strength of coordination was measured as the divergence between the measured activity pattern and surrogate data in which pairwise correlations and higher-order structure are removed by jittering—an approach that makes no assumptions about the statistics of the population responses. Our analysis shows that enhanced V1 coordination is followed several milliseconds later by spiking in the middle layers of V2, but not in further downstream V2 neurons, providing strong constraints on the proposed regimes for corticocortical signaling.

Our experimental approach was inspired in part by previous work in which the lateral geniculate nucleus (LGN) and V1 were recorded simultaneously (Reid and Alonso, 1995; Alonso et al., 1996). Like us, these studies found precise retinotopic alignment to be critical for observing tight functional coupling between upstream and downstream pairs (Reid and Alonso, 1995). LGN-V1 coupling was evident in asymmetric CCG peaks, with a peak offset of 0.9–4.5 ms (Tanaka, 1983; Reid and Alonso, 1995), similar to the latency we observed for signals between V1 and V2. LGN-V1 studies also found that synchronous spikes in thalamic pairs were more effective in driving V1 than predicted from the sum of the individual neuronal contributions, suggesting supralinear V1 summation of synaptic input (Alonso et al., 1996; see also Roy and Alloway, 2001). Our study suggests that such

observations need to be interpreted with caution: when a synchronous event is observed in a neuronal pair, this will likely involve additional, synchronous spikes in unrecorded cells (see also Yu and Ferster, 2013). Thus, the enhanced efficacy of a synchronous event could reflect simple linear summation of a broader, correlated pool, rather than a synergistic effect of synchronous input on the downstream neuron. In any case, our simulations (Figure 8) revealed that the enhanced V1 coordination associated with V2 spiking did not require special nonlinear summation downstream—our results could be recapitulated by integrate-and-fire neurons in the fluctuation-driven regime.

Limitation and Interpretation

Our results capture the relationship between V2 spiking and V1 coordination when these networks are driven by sinusoidal grating stimuli, and recorded in anesthetized animals. Anesthesia is likely to alter the strength of coordination (Kohn et al., 2009), although it seems primarily to inflate long timescale rather than the brief timescale coordination, which is well-documented in awake animals and our focus here (Cohen and Kohn, 2011). The high contrast gratings we used are effective at driving neurons in both V1 and V2. Further, the signals from V1 must be relayed to higher cortex to support perceptual awareness (Crick and Koch, 1998). Thus, these stimuli provide a useful way to determine the role of network coordination in corticocortical signaling. Other visual stimuli, by providing different patterns of network activation, might result in signaling regimes that show a different dependence on V1 coordination. However, our work clearly establishes that downstream spiking in a physiologically intact cortical network, driven with sensory input, is sensitive to coordination in a source population.

Unlike some previous work using divergence to quantify population activity (Berkes et al., 2011), we did not preserve the identity of which neurons fired in each epoch (i.e., defining population "words"). Extending our approach to include this information might be useful for revealing which activity patterns among specific subsets of V1 neurons are most relevant for driving a particular V2 cell. However, current evidence suggests that the probability of observing specific patterns of cortical activity is well approximated by considering the underlying neuronal firing rates and strength of population coordination, as we have done (Okun et al., 2012). Further, accurately measuring distributions of 100 neuron-length words may be difficult, even with the long recording periods we have used.

We attribute the relationship between V2 spiking and V1 coordination to stronger drive provided by the V1 network when its activity is more strongly coordinated. Could the relationship instead reflect drive provided by some other source, which enhances V1 coordination and, separately, causes V2 to spike? This is unlikely for several reasons. First, the relationship we observed was maximal at precisely the expected temporal delay for signals from V1 to V2, given previous measurements of the conduction velocity of the feedforward V1-V2 pathway (Girard et al., 2001; El-Shamayleh et al., 2013). Second, the primary source of shared input to V1 and V2 is feedback from higher visual cortex. These connections avoid the middle layers (Felleman and Van Essen, 1991), where we find the strongest interareal relationship. In addition, feedback projections are diffuse

(Angelucci and Bressloff, 2006), and would not be expected to generate the strong retinotopic specificity we observed. Importantly, in the monkey, V2 receives little input from the LGN (Bullier and Kennedy, 1983) and is highly dependent on V1 activity for its function (Girard and Bullier, 1989). Thus, feedforward input from the LGN, with differential delays, is not a plausible explanation for our results.

An alternative concern is that our recordings measured the activity of a small proportion of the V1 inputs to V2, and this undersampling could influence our results. However, precisely because V1 responses are coordinated, the activity we measured is indicative of spiking in other, unmonitored V1 cells. In this sense, the recorded population is simply a sample that allows us to detect coordinated spiking events in a more distributed V1 population. Consistent with this view, our simulations (Figure 8C) showed that monitoring nonprojection neurons can reveal the role of coordination in signaling, if the monitored neurons are strongly correlated with those providing drive to the downstream network. Note, however, that because brief timescale correlation has a limited spatial extent in V1 (Smith and Kohn, 2008), the firing of downstream V2 neurons with offset spatial receptive fields was not related to the strength of V1 coordination (Figures 7C and 7F). We cannot rule out the possibility that coordination in a specific, small subset of V1 neurons (not captured in our sample) would result in a stronger relationship than we observed. However, our approach was sufficiently sensitive to show a substantial elevation in V1 coordination prior to spiking in the middle layers of V2, yet failed to reveal this relationship in deeper stages of V2 processing. Thus, our results show a clear weakening of the relationship between V1 coordination and the spiking in more distant, indirect target networks.

It is important to note that the absence of a relationship between the strength of V1 coordination and the spiking in the superficial and deep layers of V2 does not indicate that coordination has no role in relaying signals across other stages of the visual system—for instance, from the middle layers of V2, where spiking coordination is robust (Smith et al., 2013), to the superficial layers. Our recording arrangement was not suitable for studying whether coordination influenced signaling between layers of V2, as we did not sample from large populations of retinotopically aligned V2 cells distributed across layers. Nevertheless, our data do provide some evidence that the spiking of V2 neurons outside the middle layers was associated with elevated coordination within the middle layers of V2 (Figure S5).

Implications

Much recent work has shown that network coordination varies with arousal, attention, learning, and stimulus drive (Kohn et al., 2009; Cohen and Kohn, 2011). The functional importance of such flexible coordination has typically been evaluated by considering its influence on the encoding or decoding of sensory information (Singer and Gray, 1995; Averbeck et al., 2006). Ultimately, however, the functional importance of network coordination must lie in how it influences the computations performed in downstream networks. Our findings suggest that changes in network coordination provide a way to alter the efficacy of the signals relayed downstream, a requirement for influencing downstream computation. Importantly, our results also

rule out "synfire" signaling in which "spike packets" are transferred faithfully across networks. Such a scheme is highly effective for relaying signals, but it leaves little room for computation (Shadlen and Newsome, 1998)—the output of the network is identical to its input, reducing it to a relay. Our data suggest corticocortical signaling works in an intermediate regime, in which coordination can dynamically modulate the efficacy of signals provided to the downstream network, without providing such potent input that downstream networks slavishly follow those inputs.

EXPERIMENTAL PROCEDURES

Physiology

We recorded from nine hemispheres of seven anesthetized paralyzed adult male monkeys (*M. fascicularis*), using procedures described previously (Smith and Kohn 2008). In brief, animals were premedicated with atropine sulfate (0.05 mg/kg) and diazepam (1.5 mg/kg). Anesthesia was induced with ketamine (10 mg/kg). During recording, anesthesia was maintained by sufentanil citrate (typically 6–18 μg/kg/hr, adjusted as needed for each animal). To minimize eye movements, the animal was paralyzed with vecuronium bromide (0.15 mg/kg/hr). Vital signs (EEG, ECG, blood pressure, SpO_2, end-tidal CO_2, temperature, and lung pressure) were monitored continuously. The pupils were dilated with topical atropine and the corneas protected with gas-permeable hard contact lenses. Refraction was provided by supplementary lenses. Experiments typically lasted 6–7 days. All procedures were approved by the Institutional Animal Care and Use Committee of the Albert Einstein College of Medicine.

We recorded neuronal activity in V1 with a 10 × 10 grid of silicon microelectrodes (1 mm length; 400 μm spacing; Blackrock). V1 receptive fields were within 2°–4° of the fovea. V2 recordings were performed with seven platinum-tungsten microelectrodes and tetrodes (300 μm spacing; Thomas Recording), advanced in the parasagital plane either vertically or angled slightly (∼15°) in the anterior direction. With this configuration, the electrodes first passed through V1 and the white matter (WM) separating V1 from V2; entry into the deep layers of V2 was evident from the reappearance of neuronal units. V1 data were recorded in 10 array implants; V2 data were obtained from 16 electrode penetrations and 55 V2 recording sites. In some penetrations we recorded at equally-spaced locations spanning V2 cortex; in others, we targeted middle-layer sites where V1-V2 functional coupling was most evident.

Waveform segments that exceeded a voltage threshold were digitized and sorted offline (Plexon). To quantify recording quality, we computed the signal-to-noise ratio (SNR) of each unit as the ratio of the average waveform amplitude to the SD of the waveform noise (Kelly et al., 2007). Only units with an SNR of 2 or greater were analyzed, corresponding to single units and groupings of several units. In addition, we removed units with firing rates less than 0.5 spikes/s (sp/s) averaged across all stimuli, as these provided too few spikes to compute accurate CCGs.

To allow histological confirmation of the recording site, we made electrolytic lesions with some V2 electrodes (2 μA for 2–10 s). Monkeys were euthanized with sodium pentobarbital and perfused with PBS followed by 10% formalin. Sections (60 μm) were stained for Nissl substance.

Visual Stimuli

We mapped the receptive field location and size of each unit using brief presentations of small gratings (0.6° in size; 250 ms presentation duration) at a range of spatial locations. RF diameter was defined as ±2 SD of a 2D-Gaussian function fit to these data. We then centered our stimuli on the aggregate receptive field of the recorded units. We presented gratings (1 cycle/deg, drift rate of 3–6.5 Hz) of 8 different orientations (22.5° interval) in a pseudorandom sequence, on a linearized CRT monitor with 1,024 × 768 pixels resolution at 100 Hz. Stimuli were viewed binocularly, at a distance of 110 cm. When the two eyes were not well-aligned, two identical gratings were presented at two locations to cover the fields of each eye. Each stimulus was presented 300–400 times (duration 1.28 s, 1.5 s interval).

Pairwise V1-V2 Analysis

We represented the spike train of each cell as a binary time series with 0.1 ms resolution and calculated cross-correlograms between V1 and V2 cells as

$$CCG(\tau) = \frac{\frac{1}{M}\sum_{i=1}^{M}\sum_{t=1}^{N}x_1^i(t)x_2^i(t+\tau)}{\Theta(\tau)\lambda_1} \qquad \text{(Equation 1)}$$

where M is the number of trials, N is the number of bins in the trial, x_1^i and x_2^i are the spike trains of a neuron in V1 and V2 on trial i, τ is the time lag, and λ_1 is the firing rate of the V1 cell. $\Theta(\tau)$ is a triangular function, $\Theta(\tau) = T - |\tau|$, where T is the trial duration in seconds, which corrects for the degree of overlap of two spike trains for each time lag. CCGs were calculated separately for each stimulus, shuffle-corrected for stimulus-locked correlations, and then combined. The jitter-corrected CCG was created by subtracting the expected value of CCGs produced from a resampled ("jittered") version of the original dataset (Smith and Kohn, 2008). Jitter-corrected CCGs were smoothed using a Gaussian kernel (SD = 1.5 ms).

A V1-V2 pair was deemed functionally connected when the jitter-corrected CCG peak height (within 10 ms of zero time lag) exceeded 5 SDs of the noise level in the CCG flanks (±75–125 ms). V2 sites were deemed to receive direct input from V1 if the average V1-V2 CCG at that site contained a significant peak, by the same definition. We computed site-average CCGs separately for each V2 electrode, to allow for the possibility that the electrodes were not uniformly positioned in V2.

Divergence Analysis

To determine the relationship between V2 activity and the degree of V1 coordination, we first determined the proportion of V1 units that were active (in a 1 ms time window) around the time of each V2 spike (±15 ms). We compared the resultant distributions with those calculated from surrogate data, in which we jittered the V1 responses (jitter windows of 5–1,280 ms, with the first window beginning at response onset). For both raw and jittered distributions, we defined response onset as 50 ms after stimulus onset (to account for V1 response latency). We analyzed responses from this time point to the end of the stimulus presentation.

To quantify the difference between the measured and jittered distributions, we used the Jensen-Shannon divergence, D_{JS},

$$D_{JS}(P \| Q) = \frac{1}{2}D_{KL}(P \| M) + \frac{1}{2}D_{KL}(Q \| M), \qquad \text{(Equation 2)}$$

where P was the distribution from raw data, Q was the distribution from jittered data, $M = \frac{1}{2}(P+Q)$, and D_{KL} is the Kullback-Leibler divergence:

$$D_{KL}(P \| Q) = \sum_i P(i)\log\left(\frac{P(i)}{Q(i)}\right). \qquad \text{(Equation 3)}$$

D_{JS} is a symmetrized version of D_{KL} that has the advantage of always having a finite value. The measured divergence depends on the number of neurons and epochs considered. For instance, if few epochs are used, so that the response distributions are poorly defined, the divergence will be inflated. To ensure a fair comparison, we chose the same number of control epochs as those associated with V2 spiking.

Simulations

The FFNs of Figure 1 used an architecture and parameters identical to Diesmann et al. (1999). Briefly, we generated a ten-layer network in which all neurons received 20,000 Poisson inputs: 12% were inhibitory and fired at 12.5 sp/s, and 88% were excitatory firing and fired at 2 sp/s. Each neuron was modeled as a leaky, integrate-and-fire neuron (see Supplemental Experimental Procedures for equations and parameters). Each layer of the network contained 100 neurons. The neurons in layers two through ten received excitatory input from cells in the preceding layer (in addition to Poisson inputs), whose number we varied to implement different convergence regimes (40, 70, 100, with only the latter used in Diesmann et al., 1999). Coordinated epochs were modeled by near-synchronous spiking (standard deviation 2.5 ms, so the packet width—3 SDs—was ~15 ms) in all the cells in the first layer. These epochs occurred randomly at a mean rate of 2 Hz.

The responses of Figure 2 (n = 100 cells) were generated by drawing samples from a mulitvariate Normal distribution and then thresholding. This approach produces spike trains constrained by user-defined first- and second-order statistics, but with a response distributions that otherwise approximates a maximum entropy distribution (Macke et al., 2009). We generated correlations similar to those seen in V1 by modifying this algorithm to produce a temporally correlated Gaussian time series (see Figure S6). Note that these simulated responses were used only to provide intuition; they were not used in the data analysis itself.

In Figure 8 we modeled a downstream V2 neuron as a leaky, integrate-and-fire cell (identical to the simulated neurons of Figure 1). The cell received input from 1,500 excitatory and 1,140 inhibitory cells, each firing at 20 sp/s. The majority of these inputs were Poisson, but a subset was chosen from a pool of 500 correlated "V1" neurons (mean pairwise correlations of 0.1 and rate of 20 sp/s). Each of the scenarios involved a distinct subset of the correlated V1 population, as further described in Supplemental Experimental Procedures.

REFERENCES

Abeles, M. (1991). Corticonics: Neural Circuits of the Cerebral Cortex (New York: Cambridge University Press).

Alonso, J.M., Usrey, W.M., and Reid, R.C. (1996). Precisely correlated firing in cells of the lateral geniculate nucleus. Nature *383*, 815–819.

Angelucci, A., and Bressloff, P.C. (2006). Contribution of feedforward, lateral and feedback connections to the classical receptive field center and extra-classical receptive field surround of primate V1 neurons. Prog. Brain Res. *154*, 93–120.

Averbeck, B.B., Latham, P.E., and Pouget, A. (2006). Neural correlations, population coding and computation. Nat. Rev. Neurosci. *7*, 358–366.

Berkes, P., Orbán, G., Lengyel, M., and Fiser, J. (2011). Spontaneous cortical activity reveals hallmarks of an optimal internal model of the environment. Science *331*, 83–87.

Bosman, C.A., Schoffelen, J.M., Brunet, N., Oostenveld, R., Bastos, A.M., Womelsdorf, T., Rubehn, B., Stieglitz, T., De Weerd, P., and Fries, P. (2012). Attentional stimulus selection through selective synchronization between monkey visual areas. Neuron *75*, 875–888.

Bruno, R.M., and Sakmann, B. (2006). Cortex is driven by weak but synchronously active thalamocortical synapses. Science 312, 1622–1627.

Bullier, J., and Kennedy, H. (1983). Projection of the lateral geniculate nucleus onto cortical area V2 in the macaque monkey. Exp. Brain Res. 53, 168–172.

Cardin, J.A., Kumbhani, R.D., Contreras, D., and Palmer, L.A. (2010). Cellular mechanisms of temporal sensitivity in visual cortex neurons. J. Neurosci. 30, 3652–3662.

Cohen, M.R., and Kohn, A. (2011). Measuring and interpreting neuronal correlations. Nat. Neurosci. 14, 811–819.

Crick, F., and Koch, C. (1998). Consciousness and neuroscience. Cereb. Cortex 8, 97–107.

Diesmann, M., Gewaltig, M.O., and Aertsen, A. (1999). Stable propagation of synchronous spiking in cortical neural networks. Nature 402, 529–533.

El-Shamayleh, Y., Kumbhani, R.D., Dhruv, N.T., and Movshon, J.A. (2013). Visual response properties of V1 neurons projecting to V2 in macaque. J. Neurosci. 33, 16594–16605.

Felleman, D.J., and Van Essen, D.C. (1991). Distributed hierarchical processing in the primate cerebral cortex. Cereb. Cortex 1, 1–47.

Fries, P. (2009). Neuronal gamma-band synchronization as a fundamental process in cortical computation. Annu. Rev. Neurosci. 32, 209–224.

Gabernet, L., Jadhav, S.P., Feldman, D.E., Carandini, M., and Scanziani, M. (2005). Somatosensory integration controlled by dynamic thalamocortical feed-forward inhibition. Neuron 48, 315–327.

Girard, P., and Bullier, J. (1989). Visual activity in area V2 during reversible inactivation of area 17 in the macaque monkey. J. Neurophysiol. 62, 1287–1302.

Girard, P., Hupé, J.M., and Bullier, J. (2001). Feedforward and feedback connections between areas V1 and V2 of the monkey have similar rapid conduction velocities. J. Neurophysiol. 85, 1328–1331.

Goldman, M.S. (2009). Memory without feedback in a neural network. Neuron 61, 621–634.

Gregoriou, G.G., Gotts, S.J., Zhou, H., and Desimone, R. (2009). High-frequency, long-range coupling between prefrontal and visual cortex during attention. Science 324, 1207–1210.

Jahnke, S., Memmesheimer, R.M., and Timme, M. (2013). Propagating synchrony in feed-forward networks. Front. Comput. Neurosci. 7, 153.

Jia, X., Smith, M.A., and Kohn, A. (2011). Stimulus selectivity and spatial coherence of gamma components of the local field potential. J. Neurosci. 31, 9390–9403.

Jia, X., Tanabe, S., and Kohn, A. (2013). γ and the coordination of spiking activity in early visual cortex. Neuron 77, 762–774.

Kelly, R.C., Smith, M.A., Samonds, J.M., Kohn, A., Bonds, A.B., Movshon, J.A., and Lee, T.S. (2007). Comparison of recordings from microelectrode arrays and single electrodes in the visual cortex. J. Neurosci. 27, 261–264.

Kohn, A., Zandvakili, A., and Smith, M.A. (2009). Correlations and brain states: from electrophysiology to functional imaging. Curr. Opin. Neurobiol. 19, 434–438.

Kremkow, J., Perrinet, L.U., Masson, G.S., and Aertsen, A. (2010). Functional consequences of correlated excitatory and inhibitory conductances in cortical networks. J. Comput. Neurosci. 28, 579–594.

Kuhn, A., Aertsen, A., and Rotter, S. (2003). Higher-order statistics of input ensembles and the response of simple model neurons. Neural Comput. 15, 67–101.

Kumar, A., Rotter, S., and Aertsen, A. (2008). Conditions for propagating synchronous spiking and asynchronous firing rates in a cortical network model. J. Neurosci. 28, 5268–5280.

Kumar, A., Rotter, S., and Aertsen, A. (2010). Spiking activity propagation in neuronal networks: reconciling different perspectives on neural coding. Nat. Rev. Neurosci. 11, 615–627.

Litvak, V., Sompolinsky, H., Segev, I., and Abeles, M. (2003). On the transmission of rate code in long feedforward networks with excitatory-inhibitory balance. J. Neurosci. 23, 3006–3015.

Long, M.A., Jin, D.Z., and Fee, M.S. (2010). Support for a synaptic chain model of neuronal sequence generation. Nature 468, 394–399.

Macke, J.H., Berens, P., Ecker, A.S., Tolias, A.S., and Bethge, M. (2009). Generating spike trains with specified correlation coefficients. Neural Comput. 21, 397–423.

Mehring, C., Hehl, U., Kubo, M., Diesmann, M., and Aertsen, A. (2003). Activity dynamics and propagation of synchronous spiking in locally connected random networks. Biol. Cybern. 88, 395–408.

Nowak, L.G., Munk, M.H., James, A.C., Girard, P., and Bullier, J. (1999). Cross-correlation study of the temporal interactions between areas V1 and V2 of the macaque monkey. J. Neurophysiol. 81, 1057–1074.

Okun, M., Yger, P., Marguet, S.L., Gerard-Mercier, F., Benucci, A., Katzner, S., Busse, L., Carandini, M., and Harris, K.D. (2012). Population rate dynamics and multineuron firing patterns in sensory cortex. J. Neurosci. 32, 17108–17119.

Ratté, S., Hong, S., De Schutter, E., and Prescott, S.A. (2013). Impact of neuronal properties on network coding: roles of spike initiation dynamics and robust synchrony transfer. Neuron 78, 758–772.

Reid, R.C., and Alonso, J.M. (1995). Specificity of monosynaptic connections from thalamus to visual cortex. Nature 378, 281–284.

Renart, A., de la Rocha, J., Bartho, P., Hollender, L., Parga, N., Reyes, A., and Harris, K.D. (2010). The asynchronous state in cortical circuits. Science 327, 587–590.

Reyes, A.D. (2003). Synchrony-dependent propagation of firing rate in iteratively constructed networks in vitro. Nat. Neurosci. 6, 593–599.

Roberts, M.J., Lowet, E., Brunet, N.M., Ter Wal, M., Tiesinga, P., Fries, P., and De Weerd, P. (2013). Robust gamma coherence between macaque V1 and V2 by dynamic frequency matching. Neuron 78, 523–536.

Rockland, K.S., and Virga, A. (1990). Organization of individual cortical axons projecting from area V1 (area 17) to V2 (area 18) in the macaque monkey. Vis. Neurosci. 4, 11–28.

Roe, A.W., and Ts'o, D.Y. (1999). Specificity of color connectivity between primate V1 and V2. J. Neurophysiol. 82, 2719–2730.

Roy, S.A., and Alloway, K.D. (2001). Coincidence detection or temporal integration? What the neurons in somatosensory cortex are doing. J. Neurosci. 21, 2462–2473.

Salazar, R.F., Dotson, N.M., Bressler, S.L., and Gray, C.M. (2012). Content-specific fronto-parietal synchronization during visual working memory. Science 338, 1097–1100.

Salinas, E., and Sejnowski, T.J. (2000). Impact of correlated synaptic input on output firing rate and variability in simple neuronal models. J. Neurosci. 20, 6193–6209.

Salinas, E., and Sejnowski, T.J. (2001). Correlated neuronal activity and the flow of neural information. Nat. Rev. Neurosci. 2, 539–550.

Schmid, M.C., Panagiotaropoulos, T., Augath, M.A., Logothetis, N.K., and Smirnakis, S.M. (2009). Visually driven activation in macaque areas V2 and V3 without input from the primary visual cortex. PLoS ONE 4, e5527.

Schwartz, O., Pillow, J.W., Rust, N.C., and Simoncelli, E.P. (2006). Spike-triggered neural characterization. J. Vis. 6, 484–507.

Shadlen, M.N., and Newsome, W.T. (1998). The variable discharge of cortical neurons: implications for connectivity, computation, and information coding. J. Neurosci. 18, 3870–3896.

Singer, W., and Gray, C.M. (1995). Visual feature integration and the temporal correlation hypothesis. Annu. Rev. Neurosci. 18, 555–586.

Smith, M.A., and Kohn, A. (2008). Spatial and temporal scales of neuronal correlation in primary visual cortex. J. Neurosci. 28, 12591–12603.

Smith, M.A., Jia, X., Zandvakili, A., and Kohn, A. (2013). Laminar dependence of neuronal correlations in visual cortex. J. Neurophysiol. 109, 940–947.

Tanaka, K. (1983). Cross-correlation analysis of geniculostriate neuronal relationships in cats. J. Neurophysiol. 49, 1303–1318.

van Kerkoerle, T., Self, M.W., Dagnino, B., Gariel-Mathis, M.A., Poort, J., van der Togt, C., and Roelfsema, P.R. (2014). Alpha and gamma oscillations characterize feedback and feedforward processing in monkey visual cortex. Proc. Natl. Acad. Sci. USA *111*, 14332–14341.

Vogels, T.P., and Abbott, L.F. (2005). Signal propagation and logic gating in networks of integrate-and-fire neurons. J. Neurosci. *25*, 10786–10795.

Wang, H.P., Spencer, D., Fellous, J.M., and Sejnowski, T.J. (2010). Synchrony of thalamocortical inputs maximizes cortical reliability. Science *328*, 106–109.

Wehr, M., and Zador, A.M. (2003). Balanced inhibition underlies tuning and sharpens spike timing in auditory cortex. Nature *426*, 442–446.

Yu, J., and Ferster, D. (2013). Functional coupling from simple to complex cells in the visually driven cortical circuit. J. Neurosci. *33*, 18855–18866.